PULSAR WIND NEBULAE IN SUPERNOVA REMNANTS

Blondin et al.

North Carolina State University

ABSTRACT

The

Subject headings: ISM: supernova remnants — shock waves — stars: pulsars: general

1. INTRODUCTION

Pulsars are expected to be born inside massive stars, so that the evolution of the wind nebulae that they produce is expected to depend on a number of different factors: the structure of the supernova, the nature of the surrounding medium, the evolution of the pulsar spin-down power, and the space velocity of the pulsar. Reynolds & Chevalier (1984) divided the evolution of pulsar nebulae into six phases that are important for their observational appearance. In phase I (~ 0 – 10^2 yr), most of the synchrotron radiation from the pulsar nebula is absorbed by the surrounding expanding supernova. Free-free absorption is important for the radio emission and photoabsorption for the X-rays. During phase II ($\sim 10^2$ – 10^3 yr), the supernova has become optically thin to the synchrotron radiation and the pulsar provides an approximately constant power. The pulsar nebula expands within the freely expanding supernova with a relatively small acceleration at the outer edge. In phase III ($\sim 10^3$ – 10^4 yr), the power input from the pulsar drops steeply so that the nebula expands adiabatically. The expansion approaches free expansion within the supernova. Phase IV ($\sim 10^4$ – 10^5 yr) begins once the reverse shock of the supernova remnant makes its way back to the center. The pulsar then finds itself in a higher pressure region and the edge of the nebula moves at a substantially slower velocity. If the pulsar has a velocity of 100's of km s^{-1}, as is quite likely for a normal pulsar (), a bow shock nebula can form around the pulsar. Phase V ($\sim 10^5$ yr) is a relatively brief phase that occurs when the pulsar wind interacts with the dense shell of the radiative supernova remnant (Shull, Fesen, & Saken 1989). The pulsar then leaves the SNR and interacts with the interstellar medium in phase VI ($\geq 10^5$ yr). The appearance of the pulsar wind nebula then depends on the nature of the interstellar medium through which it is moving.

The best studied pulsar nebula, the Crab Nebula, is probably in phase II or III. Jun (1998) has carried out numerical simulations relevant to these early phases. However, there is an increasing number of composite supernova remnants in which there is a well-developed shell remnant as well as a pulsar wind nebula; these are candidates for being in phase IV or later. The near, and best studied example of these remnants, is the Vela supernova remnant. Bock, Turtle, & Green (1998) have presented detailed radio images of the Vela pulsar nebula showing irregular filamentary structure.

The fact that the pulsar is not at the center of the radio nebula suggests that the interaction with the surroundings has been important. The *ASCA* observatory, with its capability of imaging at moderately hard X-ray energies, has found a number of pulsar nebulae inside shells, including W44 ()...

Reynolds & Chevalier (1984) made some approximate estimates of the effects of crushing a pulsar nebula by the external supernova remnant, with an emphasis on the synchrotron luminosity. Our aim here is to investigate the hydrodynamics of the interaction, with attention to instabilities. In § 2, we present the basic parameters that are needed to model the pulsar nebula/supernova remnant interaction. Numerical simulations in one and two dimensions are presented in § 3 and § 4, respectively.

2. A MODEL FOR THE PN/SNR INTERACTION

To investigate the dynamical evolution of the pulsar nebula/supernova remnant system in phase II and beyond, we have constructed a simple model based on the expanding pulsar bubble solution (Chevalier 1977) and the self-similar driven wave (Chevalier 1982). We begin by assuming the stellar material ejected by the type II supernova is expanding ballistically ($r = vt$) and can be described by a truncated power law parameterized by the total mass of ejecta, M_{ej}, the kinetic energy released in the supernova, E_{sn}, and the density power law exponent, n:

$$\rho_{ej}(r,t) = \begin{cases} \rho_t v_{pl}^n r^{-n} t^{n-3} & \text{for} \quad r > v_t t \\ \rho_t t^{-3} & \text{for} \quad r < v_t t \end{cases} \tag{1}$$

where the constant ρ_t is given by

$$\rho_t = \frac{5n-25}{2\pi n} E_{sn} v_t^{-5} \tag{2}$$

and the velocity at the intersection of the density plateau and the power law is given by

$$v_t = \left(\frac{10n-50}{3n-9} \frac{E_{sn}}{M_{ej}} \right)^{1/2} \tag{3}$$

If we further assume that this ejecta is expanding into a uniform ambient medium with density ρ_a, the expansion of the supernova remnant is described by a self-similar solution given by Chevalier (1982). The radius of the forward shock, R_1, in this self-similar driven wave (SSDW) is given by (assuming $s = 0$ in Chevalier's notation)

$$R_1 = A \left(\frac{\rho_t v_t^n}{\rho_a} \right)^{\frac{1}{n}} t^{\frac{n-3}{n}} \tag{4}$$

where the constant $A = 1.048$ for $n = 9$, but varies relatively little with the value of n.

The last component of the model, the pulsar wind nebula, is treated as an adiabatic wind bubble driven by a pulsar wind with a kinetic luminosity, L_p. If we use the standard approximation of an isobaric bubble bounded by a thin shell of swept up ambient gas, the expansion of this bubble within the uniform (but decreasing with time) density of the ejecta is given by

$$R_p = 1.5421 \left(\frac{n-5}{n-3}\right)^{1/4} \left(\frac{E_{sn}^3 L_p^2}{M_{ej}^5}\right)^{1/10} t^{6/5} \tag{5}$$

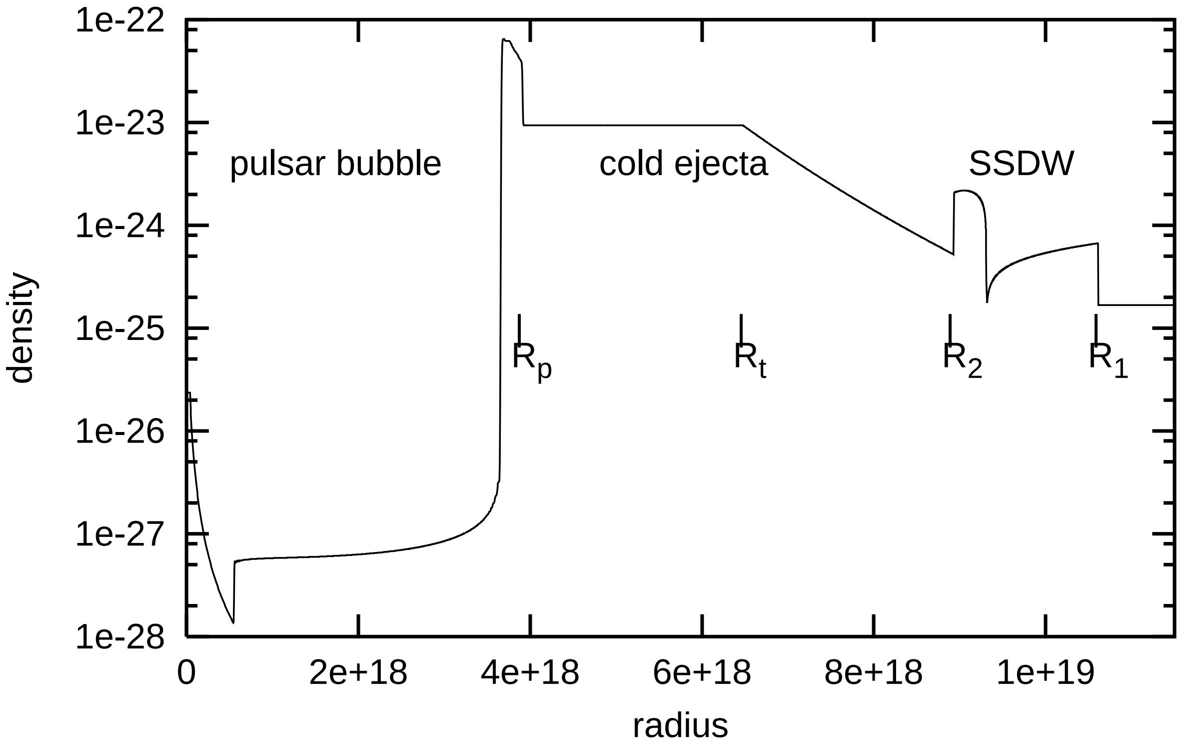

Fig. 1.— The density profile of our model for the interaction of a pulsar nebula with the host supernova remnant. The reverse shock is just about to reach r_t and begin propagating toward the center.

This combined model is illustrated in Figure 2 which shows the radial profile of the density throughout the structure. The supernova ejecta is separated into three parts: a thin shell at R_p that has been swept up by the expanding pulsar bubble, cold freely expanding ejecta between R_p and the reverse SNR shock at R_2, and a thin shell of shocked ejecta at R_2 that has been decelerated by the reverse shock. The discontinuity in between R_2 and R_1 separates the shocked ejecta (on the left) and the shocked CSM (on the right). The discontinuity near $r = 0$ is the termination shock of the pulsar wind.

Several things will happen at an age of $\sim 10^3$ years to break this model. First, the pulsar will die out. Without continued power input, the expansion of the pulsar nebula will slow down until it becomes frozen into the expanding ejecta. Second, the pulsar nebula will reach the edge of the plateau in the SN ejecta and begin accelerating down the steep density gradient. Alternatively, the plateau will reach the reverse shock of the SSDW. As the ram pressure at the reverse shock rapidly decays away, the reverse shock is driven toward the center of the remnant, resulting in a dynamical interaction with the pulsar nebula.

The exact ordering of these events depends on the parameters of the model described above, namely E_{sn}, M_{ej}, n, ρ_a, L_p and the lifetime of the pulsar, τ_{psr}. The time of the first event, the "death" of the pulsar, is simply τ_p. This age is typically of order 10^3 yrs. The second event, the pulsar nebula reaching r_t, occurs at

$$t_2 = 2.33 \left(\frac{n-5}{n-3}\right)^{5/4} \frac{E_{sn}}{L_p} \tag{6}$$

assuming constant pulsar luminosity. If, however, the pulsar has already died away, the nebula will expand slower and this will be an underestimate to t_2. The third event, the falling in of the reverse shock, begins when the edge of the ejecta plateau, $R_t = v_t * t$, reaches the reverse shock:

$$t_3 = B \left(\frac{\rho_t}{\rho_a}\right)^{1/3} \approx 120 \left(\frac{M_{ej}}{M_\odot}\right)^{5/6} \left(\frac{\rho_a}{m_p}\right)^{-1/3} \left(\frac{E_{sn}}{10^{51}\mathrm{erg}}\right)^{-1/2} \mathrm{yrs}, \tag{7}$$

where the numerical coefficient $B = 0.688$ for $n = 9$.

Choosing reasonable parameters as listed in Table 2 for Model A, we find $t_2 \approx 4,500$ yrs and $t_3 \approx 1,500$ yrs. Thus we expect the reverse shock to begin falling into the interior of the remnant where it will encounter the pulsar nebula. For other parameters, however, this sequence may be reversed. For example, lowering E_{sn} by 3 would lead to $t_2 < t_3$; the lower energy means a slower expansion, requiring a longer time to sweep up mass but a shorter time for the pulsar to blow through the slower ejecta.

3. ONE-DIMENSIONAL HYDRODYNAMIC SIMULATIONS

To investigate the dynamical evolution of the pulsar nebula from phase III through phase IV, we employ numerical simulations that begin at $t = \tau_p$. These simulations are computed with the VH-1 code, a Lagrangian-Remap version of the Piecewise Parabolic Method. The standard VH-1

Parameter	Definition	Units	Model A	Model B	Model C
E_{sn}	kinetic energy of SN	10^{51} erg	1	1	1
M_{ej}	mass of SN ejecta	$M_\odot$	8	4	16
n	ejecta power law		9	9	9
ρ_a	ambient density	m_p cm^{-3}	0.1	0.1	0.1
L_p	pulsar luminosity	10^{40} erg s^{-1}	1	0.038	6.26
τ_p	pulsar lifetime	yrs	550	500	500

code was adapted to treat two fluids with two different values of γ such that the pulsar wind can be modeled with $\gamma = 4/3$ while the supernova ejecta and circumstellar gas is modeled with $\gamma = 5/3$. The one-dimensional PN/SNR model is evolved on a grid of 750 radial zones that expands to follow the forward shock. Several simulations on a grid of 1500 zones produced almost identical results.

The initial conditions for the SSDW are taken from the solution described in Chevalier (1982), scaled to the parameters listed in Table 2 for Model A. The initial conditions for the pulsar nebula are taken from a separate hydrodynamic simulation of a wind blown bubble in which the wind is an adiabatic gas with $\gamma = 4/3$, a mass loss rate $\dot{M}_w = 2L_p/v_p^2$, and a wind velocity, v_p, scaled to yield a sound speed in the shocked gas of $c/\sqrt{3}$, appropriate for a relativistic gas.

A more realistic model for the pulsar wind nebula would allow for a relativistic, MHD (magnetohydrodynamic) flow, as in the steady state model for Crab Nebula by Kennel & Coroniti (1984). However, once the relativistic wind passes through the wind termination shock, the flow velocity drops to $c/3$. The bulk velocity is not relativistic in the nebula, although the shocked particles are highly relativistic. This situation can be approximated by a $\gamma = 4/3$ fluid. The magnetic field may be a more significant omission because the magnetic field in the Crab Nebula is thought to be in approximate equipartition with the particles. In particular, the magnetic field could affect the growth of instabilities a the edge of the pulsar nebula (Jun)

The evolution of the PN/SNR model is illustrated with a space-time diagram in Figure 3. The evolution begins shortly after τ_p, after the pulsar wind shock has collapsed, leaving behind a uniform pressure bubble. One can identify two bands of high-density gas in the early evolution: the pulsar nebula shell made up of swept up ejecta, and a shell of shell of shocked ejecta on the trailing side of the SSDW. One can also see the edge of the density plateau in the cold (low-pressure) expanding ejecta in between these two shocked-ejecta shells. From this image it is clear that the ejecta plateau reaches the reverse shock (the trailing side of the SSDW) before the pulsar shell, but the SSDW does not have much time to react to the dropping ejecta density before the pulsar shell strikes it.

At an age of about ~ 2500 years the pulsar nebula shell collides with the dense SSDW shell. From this point on all of the ejecta is contained in a relatively thin shell (width $\sim 0.1\,R_1$) bounded by low density shocked pulsar wind on the inside and by shocked circumstellar gas on the outside. This initial impact generates a strong shockwave transmitted through the SSDW. When this shock catches up with the forward shock there is an abrupt, but brief, acceleration of the forward shock, followed by a faster deceleration than in the SSDW phase. A weak reflected shock is also generated, which bounces back and forth through the pulsar bubble at the relatively high sound speed of $c/\sqrt{3}$. This bouncing wave can be seen as vertical lines in the pressure image of Figure 3.

Following the collision of the pulsar and reverse SNR shocks, the thin shell of ejecta is gradually pushed inward with respect to the outer shockwave by the high pressure of the shocked CSM, reaching a minimum radius of $0.14\,R_1$ at an age of $\sim 30,000$ years. At this point the pressure of the compressed pulsar bubble accelerates the shell of shocked ejecta back out to a radius of $0.25\,R_1$.

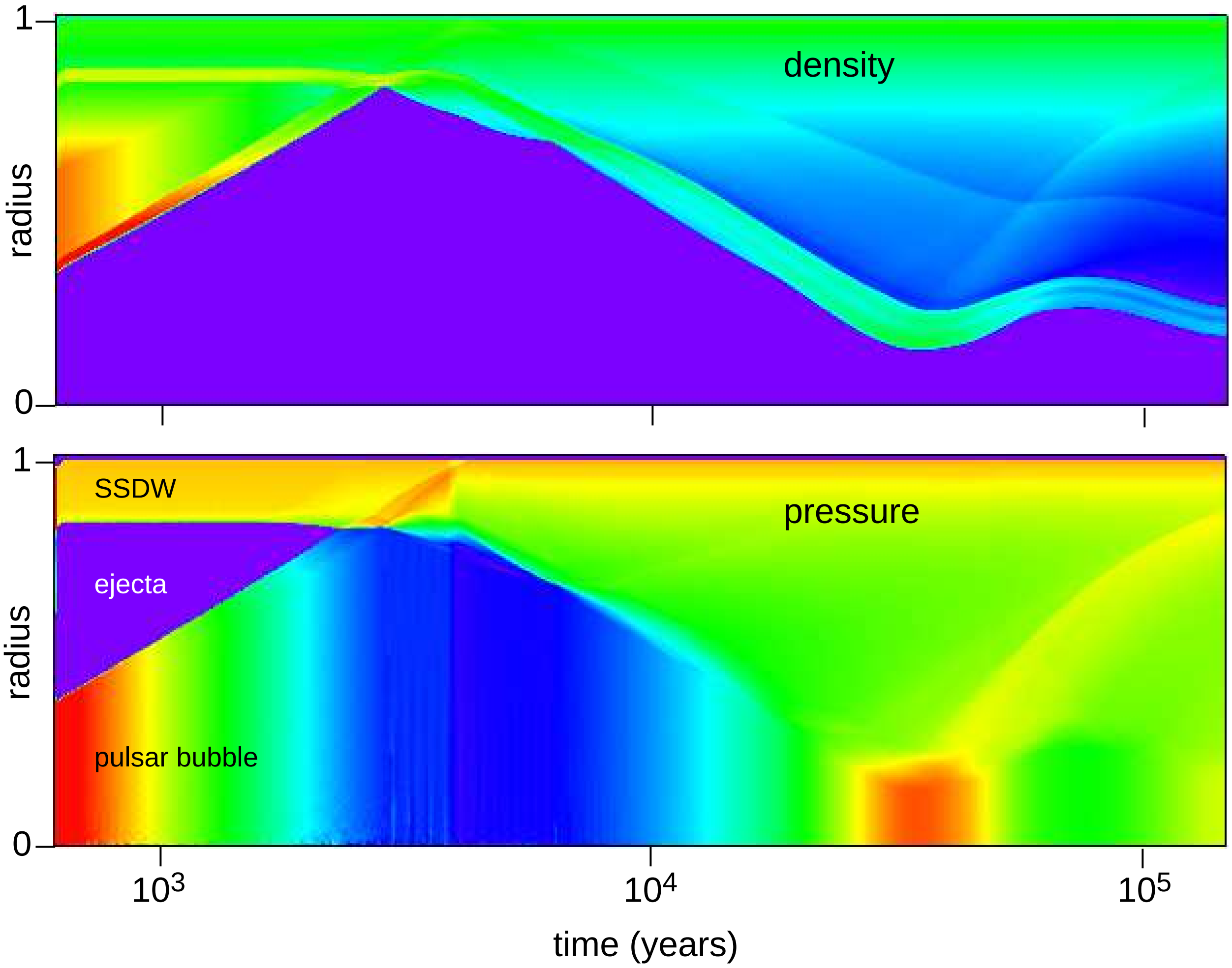

Fig. 2.— Evolution of the pulsar nebula within the host supernova remnant as computed with the one-dimensional hydrodynamics model. Both the density (top) and the pressure (bottom) are depicted in logarithmic scales, with red corresponding to high values and purple to low values. The radial extent of the grid is scaled to follow the forward shock front, such that the location of the forward shock is a horizontal line near the top of each plot. The initial conditions correspond to the density profile in Figure 1, minus the unshocked pulsar wind.

From this point on all of the ejecta remains in a thin shell with a width of $\sim 10\%$ of R_1, slowly oscillating about an average radius of $\sim 0.2\,R_1$.

The extent to which the pulsar bubble is compressed depends on the pressure in the bubble compared to the pressure behind the reverse shock as it propagates in toward the pulsar nebula. Using the pressure behind the reverse shock in the SSDW phase, we find a ratio of pressures at a time of t_3:

$$\frac{P_b}{P_2} = 0.375\, L_p^{2/5}\, M_{ej}^{1/3}\, \rho_a^{-2/15}\, E_{sn}^{-3/5}, \tag{8}$$

where the numerical coefficient is slightly dependent on the value of n (value quoted is for $n = 9$). This ratio is ~ 0.45 for our nominal parameters. Note that both of these pressures will be slightly lower; P_b because the pulsar has likely died out by the time of the collision, P_2 because the pressure in the driven wave will drop once the reverse shock starts falling to the center.

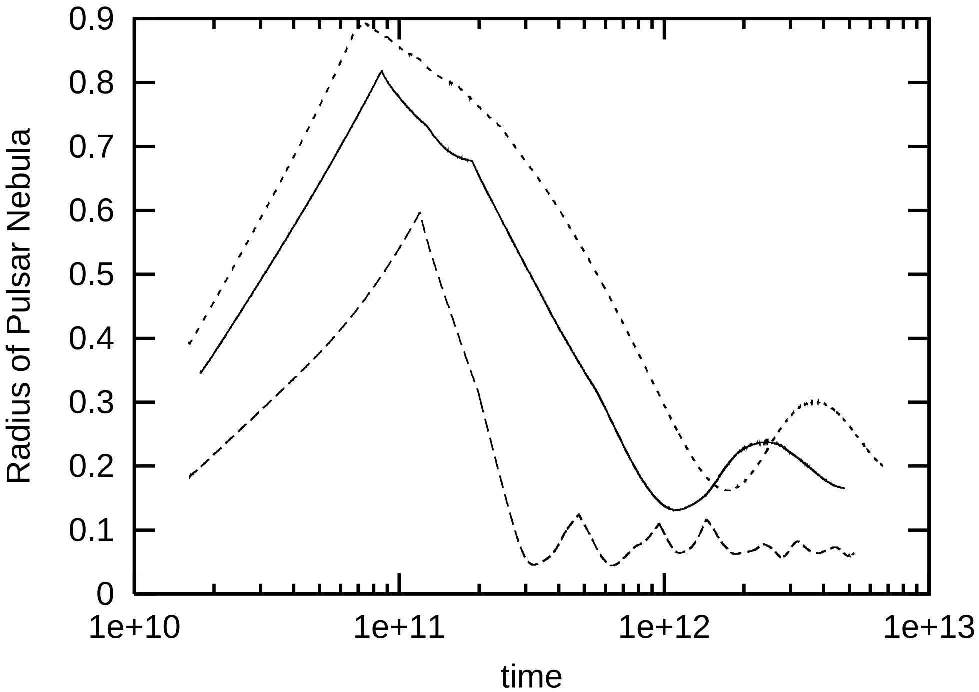

Fig. 3.— Evolution of the pulsar nebula through the crash of the reverse SNR shock for the three different models listed in Table 1: Model A (solid), Model B (short dash), and Model C (long dash). The radius of the pulsar nebula is scaled to the (increasing) radius of the SNR as in the previous figure.

We have run two other models in order to show the effects of changing the energy in the pulsar bubble on the evolution of the PN/SNR interaction. In Model B we dropped the pressure ratio in Equation 8 by a factor of 1.84 through a smaller ejecta mass ($4\ M_\odot$) and smaller pulsar luminosity (3.8×10^{38} erg s^{-1}). In Model C the pressure ratio was increased by a factor of 20.7 by doubling the ejecta mass (16 $M_\odot$) and increasing the pulsar luminosity (6.26×10^{40} erg s^{-1}). The evolution of all three models is shown in Figure 3. As expected, the lower the pressure in the pulsar bubble, the more the bubble is compressed by the reverse shock. In the lower pressure model the radius of the bubble after collapse is only $\sim 0.06\, R_1$.

The evolution in the high-pressure model is slightly different since these parameters switch the ordering of t_2 and t_3. In this case the pulsar nebula hits the edge of the ejecta plateau at $\sim \tau_p$, well before the PN/SNR collision. There is thus an intermediate phase when the pulsar shell accelerates down the steep ejecta gradient before impacting the SSDW. This results in a more violent collision, which compresses the SSDW by a factor of ~ 2 and accelerates the forward shock considerably more than in the standard model. Despite this more violent beginnin, however, the subsequent evolution is very similar to the standard model, albeit leaving behind a slightly larger pulsar bubble.

4. TWO-DIMENSIONAL HYDRODYNAMIC SIMULATIONS

To investigate the effects of these instabilities on the morphology of the pulsar nebula, we have extended our models to two dimensions. We computed these models on a cylindrical (R-z) grid of 2000 x 2000 zones. We assume reflection symmetry about the equator and compute only one hemisphere. The initial conditions are taken from the first stage of the one-dimensional simulations just after the crash of the reverse wind shock. In order to make these simulations more computationally efficient, we have raised the density in the pulsar bubble by a factor of 30. This artificially lowers the sound speed in the hot bubble allowing the use of a larger time step. Although this increases the time needed to equilibrate the pressure in the bubble, the sound crossing time is still relatively short and 1D simulations with and without this modification were almost identical. Again, we evolve this model on a moving grid that follows the outer shock front, so that the full resolution of the grid is always used.

The outer shock front remains very nearly spherical and follows the time evolution of the one dimensional model almost exactly. The key difference is instability of the thin shell of ejecta and the rapid mixing driven by this instability. Even before the PN/SNR interaction, the instability of the SSDW (Chevalier et al 1992) begins to spread out the shell of shocked ejecta, although in this simulation there is not enough time for this instability to grow to significant amplitude. Following the PN/SNR collision, the deceleration of the ejecta shell by the shocked CSM (responsible for the SSDW instability) increases in magnitude, thereby driving a more rapid Rayleigh-Taylor instability. The result is a broadened shell of mixed ejecta and CSM as seen in the first frame of Figure 4.

Much more dramatic, however, is the Rayleigh-Taylor instability working in the opposite direction when the high pressure of the compressed pulsar bubble begins to accelerate the ejecta shell back outwards. As a result of this instability, much of the ejecta mass continues toward the center of the SNR almost unabated.

As seen in Figure 4, the ejecta gas and bubble gas become well mixed by this instability on

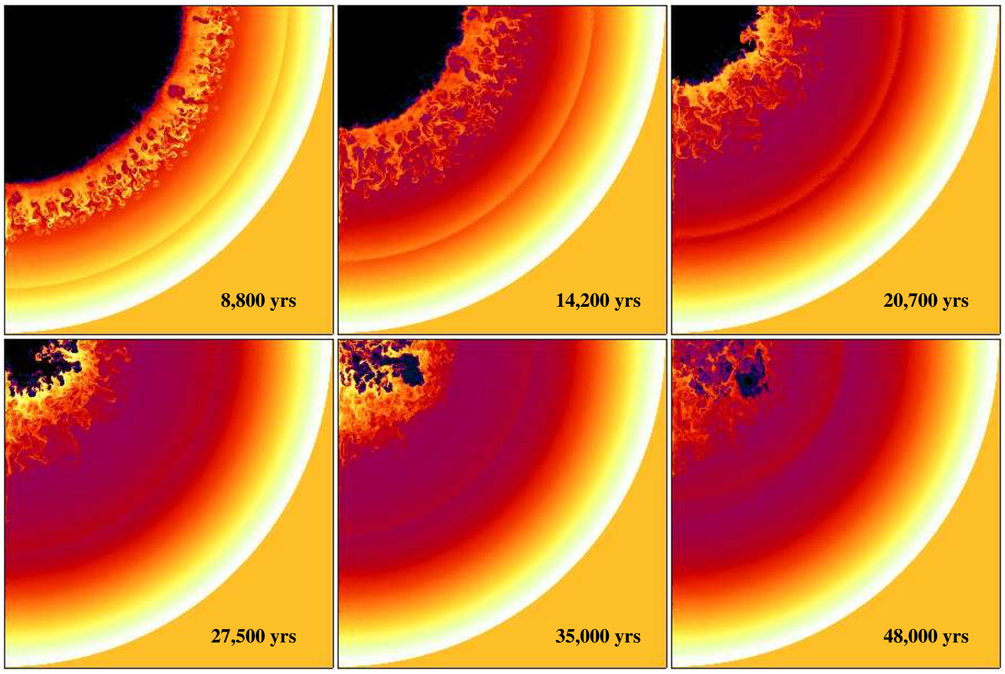

Fig. 4.— Crushing of the pulsar nebula in a two-dimensional simulation using the parameters for Model A listed in Table 1.

a time scale comparable to the bubble bounce seen in the 1D simulation. Here we plot the radius of the pulsar bubble in the 2D simulation by summing up the volume of gas with $\gamma < 1.66$ (i.e., including the partially mixed gas) and calculating an effective radius assuming a spherical volume. Prior to the bounce, the 1D and 2D simulations are almost identical, but rapid mixing of the ejecta and bubble gas following bounce quickly depletes the volume of relativistic gas. Note that this depletion is an artifact of numerical diffusion; when one numerical zone contains both bubble gas ($\gamma = 4/3$) and ejecta ($\gamma = 5/3$), the mass-weighted average γ is dominated by the high density of the ejecta.

The efficiency of this mixing is shown in Figure 4, which shows a close up of the center of the SNR at a time corresponding to the second to last frame in Figure 4. Talk about resolution effects...

5. EVOLUTION IN NONUNIFORM MEDIA

We have repeated our 2D simulation with the addition of a density gradient in the CSM, with the goal of understanding the displacement of the pulsar bubble seen in the Vela SNR. We use a

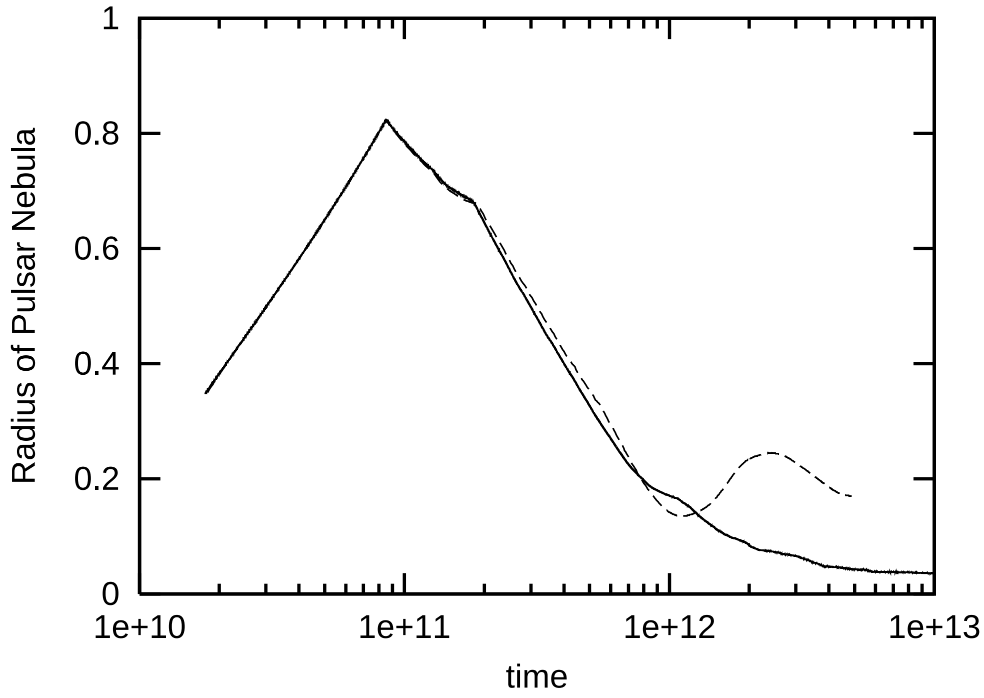

Fig. 5.— Evolution of the pulsar nebula through the crash of the reverse SNR shock in one (solid line) and two (dashed line) dimensions.

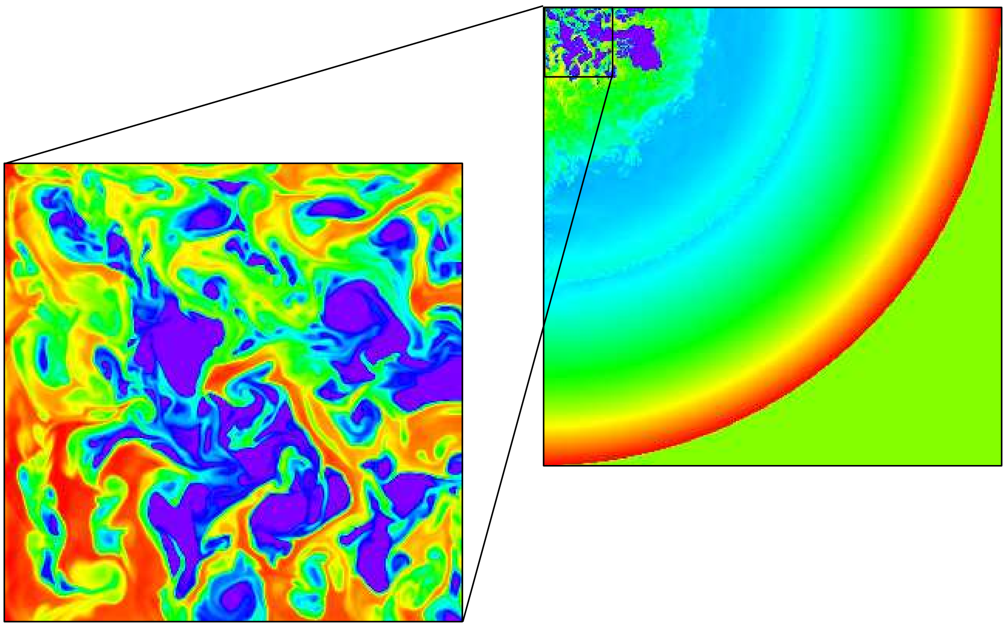

Fig. 6.— The rapid mixing of ejecta and pulsar wind is seen in this density image at a time of 1.1×10^{12} seconds, shortly after the bounce of the pulsar bubble in the corresponding one-dimensional simulation.

smooth density distribution in the vertical direction given by

$$\rho(z) = \rho_c \left[1 + \frac{2-x}{x}\tanh(z/H)\right] \tag{9}$$

such that the density contrast, from a maximum at large positive z to a minimum at large negative z, is given by $(x-1)^{-1}$, and H is the characteristic length scale over which the density changes. The simulations shown here use $x = 1.2$ corresponding to a density contrast of 5. These simulations require the computation of the full domain in z (i.e., no assumption of equatorial symmetry). As a result, or standard grid of 2000 zones represents only half the resolution used in the previous 2D model.

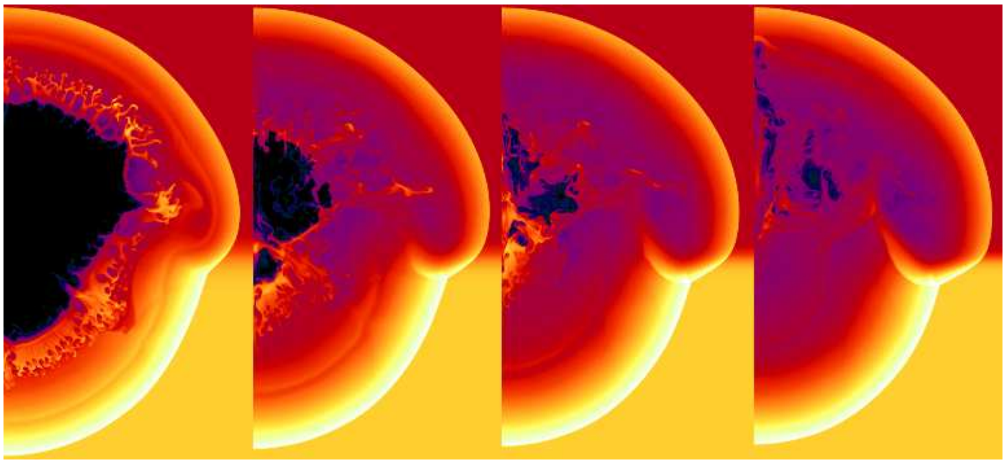

Fig. 7.— The evolution of the pulsar nebula/supernova remnant for the model with a scale height of $H = 1 \times 10^{19}$ cm in the ambient medium.

In Figure 5 we show the evolution of the PN/SNR system for a CSM length scale of $H = 1 \times 10^{19}$ cm, which corresponds to the size of the SNR at an age of $\sim$ 500 yrs. Thus, by the time of the PN/SNR collision the radius of the SNR is much larger than the characteristic scale length in the CSM, and the density variation in the CSM looks like an abrupt step function. As a result, the shape of the pulsar bubble quickly deformed once the asymmetry of the CSM is transmitted to the pulsar bubble through the PN/SNR collision.

Support for this work was provided in part by NASA grants NAG5-8130 and NAG-7153. The hydrodynamic simulations were computed on an IBM SP at the North Carolina Supercomputing Center.

REFERENCES

Angerhofer, P. E., Strom, R. G., Velusamy, T., & Kundu, M. R. 1981, A&A, 94, 313

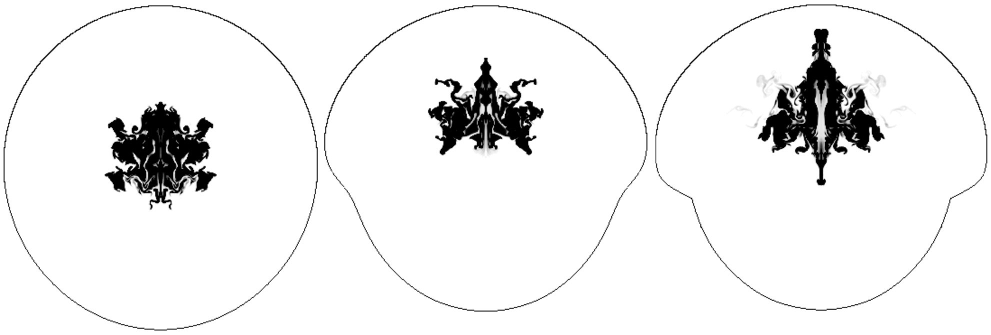

Fig. 8.— The remnants of the pulsar nebula as defined by the adiabatic index (black is gas with $\gamma < 5/3$) for simulations with a scale height of $H = 1 \times 10^{20}$ cm (left) and $H = 3 \times 10^{19}$ cm (center) and $H = 10^{19}$ cm (right). The solid contours mark the location of the shock front. These snapshots are from a time of $\sim 50,000$ years.

Atoyan, A. M. 1999, A&A, 346, L49

Bietenholz, M. F., Frail, D. A., & Hankins, T. H. 1991, ApJ, 376, L41

Bietenholz, M. F., Kassim, N., Frail, D. A., Perley, R. A., Erickson, W. C., & Hajian, A. R. 1997, ApJ, 490, 291

Bietenholz, M. F., & Kronberg, P. P. 1990, ApJ, 357, L13

Bietenholz, M. F., & Kronberg, P. P. 1992, ApJ, 393, 206

Bock, D. C.-J., Turtle, A. J., & Green, A. J. 1998, AJ, 116, 1886

Caswell, J. L., Kesteven, M. J., Komesaroff, M. M., Haynes, R. F., Milne, D. K., Stewart, R. T., & Wilson, S. G. 1987, MNRAS, 225, 329

Chevalier, R. A. 1977, in Supernovae, ed. D. N. Schramm (Dordrecht: Reidel), 53

Chevalier, R. A. 1982, ApJ, 258, 790

Crotts, A. P. S., Kunkel, W. E., & Heathcote, S. R. 1995, ApJ, 438, 724

de Jager, O. C., Harding, A. K., & Strickman, M. S. 1996, ApJ, 460, 729

Frail, D. A., Giacani, E. B., Goss, W. M., & Dubner, G. 1996, ApJ, 464, L165

Frail, D. A., & Kulkarni, S. R. 1991, Nature, 352, 785

Frail, D. A., & Scharringhausen, B. R. 1997, ApJ, 480, 364

Fruchter, A. S., Taylor, J. H., Backer, D. C., Clifton, T. R., Foster, R. S., & Wolszczan, A. 1988, Nature, 331, 53

Gaensler, B. M., Stappers, B. W., Frail, D. A., & Johnston, S. 1998, ApJ, 499, L69

Gaensler, B. M., Stappers, B. W., Frail, D. A., Moffett, D. A., Johnston, S., & Chatterjee, S. 2000, MNRAS, submitted (astro-ph/0004273)

Gallant, Y. A., & Tuffs, R. J. 2000, in Pulsar Astronomy – 2000 and Beyond, ed. M. Kramer, N. Wex, & N. Wielebinski (San Francisco: ASP), 503

Harnden, F. R., Jr., Grant, P. D., Seward, F. D., & Kahn, S. 1985, ApJ, 299, 828

Johnston, S., & Galloway, D. 1999, MNRAS, 306, L50

Jun, B.-I. 1998, ApJ, 499, 282

Jun, B.-I., Norman, M. L., & Stone, J. M. 1995, ApJ, 453, 332

Kennel, C. F., & Coroniti, F. V. 1984a, ApJ, 283, 694 (KC84a)

Kennel, C. F., & Coroniti, F. V. 1984b, ApJ, 283, 710 (KC84b)

Kovalenko, A. V., Pynzar', A. V., & Udal'tsov, V. A. 1994, Astron. Rep., 38, 95

Kronberg, P. P., Lesch, H., Ortiz, P. F., & Bietenholz, M. F. 1993, ApJ, 416, 251

Kundt, W., & Krotscheck, E. 1980, A&A, 83, 1

Manchester, R. N., Staveley-Smith, L., & Kesteven, M. J. 1993, ApJ, 411, 756

Ögelman, H. B., Koch-Miramond, L., & Aurière, M. 1989, ApJ, 342, L83

Pacini, F., & Salvati, M. 1973, ApJ, 186, 249

Plucinsky, P. P. 1998, Mem. Soc. Astron. Italia, 69, 939

Rees, M. J., & Gunn, J. E. 1974, MNRAS, 167, 1

Reynolds, S. P., & Chevalier, R. A. 1984, ApJ, 278, 630

Salter, C. J., Reynolds, S. P., Hogg, D. E., Payne, J. M., & Rhodes, P. J. 1989, ApJ, 338, 171

Shklovskii, I. S. 1977, SvA, 23, 515

Shull, J. M., Fesen, R. A., & Saken, J. M. 1989, ApJ, 860, 868

Stappers, B. W., Gaensler, B. M., & Johnston, S. 1999, MNRAS, 308, 609

Sun, M., Wang, Z.-R., & Chen, Y. 1999, ApJ, 511, 274

This preprint was prepared with the AAS LaTeX macros v5.0.